Title: **The uncoating of EV71 in mature late endosomes requires CD-M6PR**

Seii OHKA[1,2,*], Soon Hao TAN[3], Eri ISHIYAMA[4], Katsutoshi OGASAWARA[4], Tomohito HANASAKA[4], Kinji ISHIDA[4], Kyoji HAGIWARA[1], Chia-Chyi LIU[5], Pele Choi-Sing CHONG [5,6], Ken-ichi HANAKI[4,7], Giampietro SCHIAVO[8,9]

1. Neurovirology Project, Tokyo Metropolitan Institute of Medical Science, Tokyo, Japan
2. Present address: Addictive Substance Project, Tokyo Metropolitan Institute of Medical Science, Tokyo, Japan
3. Department of Pathology, University of Malaya, Kuala Lumpur, Malaysia
4. Technical Support Center for Life Science Research, Iwate Medical University, Iwate, Japan
5. National Institute of Infectious Diseases and Vaccinology, National Health Research Institutes, Zhunan Town, Miaoli County, Taiwan
6. Present address: BravoVax Co., Ltd, Wuhan, China
7. Present address: Division of Experimental Animal Research, National Institute of Infectious Diseases, Tokyo, Japan
8. Queen Square Institute of Neurology, University College London, London, United Kingdom
9. UK Dementia Research Institute at UCL, London, United Kingdom

Running title: M6PR's roles in EV71 uncoating

Document totals:	Word count for Summary statement:	21
	Word count for Abstract:	152
	Word count for main text:	7,604

*Corresponding author:
Seii OHKA
Addictive Substance Project, Tokyo Metropolitan Institute of Medical Science, 2-1-6, Kamikitazawa, Setagaya-ku, Tokyo 156-8506, Japan
Phone: +81-3-5316-2390 Fax: +81-3-5316-2390
E-mail: ohka-si@igakuken.or.jp

Keywords EV71, late endosomes, mannose 6-phosphate receptor, uncoating, SCARB2

Summary Statement

In human rhabdomyosarcoma cells overexpressing human scavenger receptor B2, EV71 uncoating takes place in mature late endosomes and relies on CD-M6PR.

Abstract

Enterovirus 71 (EV71) is one of the causative agents of hand-foot-and-mouth disease, which in some circumstances could lead to severe neurological diseases. Despite of its importance for human health, little is known about the early stages of EV71 infection. EV71 starts uncoating with its receptor, human scavenger receptor B2 (hSCARB2), at low pH. We show that EV71 was not targeted to lysosomes in human rhabdomyosarcoma cells overexpressing hSCARB2 and that the autophagic pathway is not essential for EV71 productive uncoating. Instead, EV71 was efficiently uncoated 30 minutes after infection in late endosomes (LEs) containing hSCARB2, mannose-6-phosphate receptor (M6PR), RAB9, bis(monoacylglycero)phosphate and lysosomal associated membrane protein 2 (LAMP2). Furthering the notion that mature LEs are crucial for EV71 uncoating, cation-dependent (CD)-M6PR knockdown impairs EV71 infection. Since hSCARB2 interacts with cation-independent (CI)-M6PR through M6P-binding sites and CD-M6PR also harbor a M6P-binding site, CD-M6PR is likely to play important roles in EV71 uncoating in LEs.

Introduction

Enterovirus 71 (EV71) is a causative agent of hand-foot-and-mouth disease (HFMD) in young children and infants (Hagiwara et al., 1978, Blomberg et al., 1974), yet infection with this virus occasionally leads to severe neurological diseases, such as brainstem encephalitis and acute flaccid paralysis (McMinn, 2002). EV71 is classified into *Enterovirus* within the family *Picornaviridae* (Racaniello, 2007), which contains positive-sense single-stranded RNA surrounded by an icosahedral capsid proteins. Sixty copies of the four structural proteins VP1, VP2, VP3, and VP4 assemble to form the capsid (Plevka et al., 2012, Rossmann and Johnson, 1989, Wang et al., 2012). Functional EV71 receptor, human scavenger receptor class B, member 2 (hSCARB2, also known as lysosomal integral membrane protein II or CD36b like-2) (Yamayoshi et al., 2009), interacts with residues located within an indentation of the viral capsid, called the canyon (Dang et al., 2014). After the binding of hSCARB2 to the EV71 capsid, the virus particle releases viral genomic RNA using VP1 and VP4 under acidic conditions (Yamayoshi et al., 2013, Dang et al., 2014).

hSCARB2, a CD36 family member containing two transmembrane domains (Vega et al., 1991), is an intrinsic receptor for β-glucocerebrosidase (β-GC) (Eskelinen et al., 2003). It transports β-GC from the endoplasmic reticulum (ER) to lysosomes (Blanz et al., 2010, Reczek et al., 2007), and is required for lysosomal integrity (Eskelinen et al., 2003). In primate cells, lysosome sorting of β-GC by hSCARB2 is aided by cation-independent (CI)-mannose-6-phosphate (M6P) receptor (M6PR) (Zhao et al., 2014), which binds to a M6P group linked to amino acid 325 of hSCARB2; however, cation-dependent (CD)-M6PR may also contribute to the lysosome sorting of β-GC by hSCARB2 (Zhao et al., 2014). β-GC and EV71 bind overlapping regions of the intraluminal domain of hSCARB2: β-GC interacts with the 145-222 portion of hSCARB2 (in particular 150-167) (Zachos et al., 2012, Reczek et al., 2007), whereas amino acids 142-204 (and in particular 144-151) are crucial

for EV71 binding (Chen et al., 2012, Yamayoshi and Koike, 2011).

It has been reported that small interfering RNAs (siRNAs) against clathrin heavy chain inhibit EV71 infection, suggesting that EV71 exploits a clathrin-dependent pathway for its entry into target cells (Lin et al., 2012, Hussain et al., 2011). After internalization, EV71 is delivered to early endosomes (Yamayoshi et al., 2013), however, the precise mechanism for EV71 uncoating, such as its timing and localization, has not been clarified. In the endocytic pathway, early endosomes mature to late endosomes (LEs), which then fuse with lysosomes containing lysosomal associated membrane protein (LAMP)-1 or 2. Progression along the endosomal route is regulated by specific RAB GTPases, which serve as specific markers of these organelles. RAB5 regulates the early steps in the endocytic pathway, participating to clathrin coated vesicle uncoating and formation of early endosomes (Semerdjieva et al., 2008, Pfeffer, 2017), whilst RAB7 regulates the transition between early endosomes and LEs (Wandinger-Ness and Zerial, 2014), and RAB9 functions in LEs and the trans-Golgi network (Pfeffer, 2017).

LAMP-1 and LAMP-2 are lysosomal membrane proteins, which share common functions in vivo. Beyond their roles in maintaining the structural integrity of lysosomes, both LAMPs are involved in the regulation of autophagic vacuoles and unesterified cholesterol in embryonic fibroblasts (Eskelinen, 2006). In previous studies, SCARB2 was found to co-localize with LAMP-2 in primate cells (Zachos et al., 2012).

Here, we report that EV71 is efficiently uncoated 30 minutes after infection (m.a.i.) in mature LEs. Cation-dependent (CD)-M6PR was found to be essential for EV71 replication by siRNA knockdown, suggesting that CD-M6PR may play an important role at early stages of EV71 infection.

Results

Analysis of EV71 uncoating kinetics

EV71 is uncoated upon binding to hSCARB2 at low pH (Yamayoshi et al., 2013). However, it is unclear where and when uncoating occurs in cells. To clarify when EV71 starts uncoating, we used light-sensitive EV71, which can be inactivated after irradiation at 450 nm. Human rhabdomyosarcoma RD cells overexpressing hSCARB2 (RD-hSCARB2), were infected with light-sensitive EV71 at a multiplicity of infection (MOI) of 10 and cells were either kept in the dark or irradiated at the indicated time after infection to inactivate intact virus. Seven hours after infection, cells were harvested and the viral titers were determined (Fig. 1A). In samples irradiated at either 5 or 10 m.a.i., virus titers decreased by 3 logs as compared to samples kept in the dark (Fig. 1A and 1B). In contrast, the viral titer of the sample irradiated at 20 m.a.i. was found to increase as compared to that in the 10 m.a.i. sample, and a further increase of viral titer was observed at 40 m.a.i. (Fig. 1A and 1B). The viral titer was found to plateau at 60 m.a.i., suggesting that the uncoating of EV71 is likely to start after 10 m.a.i. and that all the productive viral particles were uncoated before 40 m.a.i. The experiments were repeated three times and similar results were observed.

Next, we combined in situ hybridization and immunofluorescence to visualize the viral RNA as well as the viral capsid. RD-hSCARB2 cells were infected with purified EV71 at an MOI of 25 and cells were fixed at specific times after infection, followed by immunofluorescence and in situ hybridization (Fig. 1C). The number of EV71 genomic RNA puncta per cell were analyzed (Fig. 1D); we found 1.4, 0.9 and 3.2 for 0 m.a.i., 2.8, 4.0 and 1.3 for 10 m.a.i., 4.2, 13.5 and 7.0 for 20 m.a.i., 46.0, 30.8 and 44.9 for 30 m.a.i., 1.6 and 2.0 for 30 m.a.i. with NH_4Cl. At 0 m.a.i., we observed negligeable amounts of EV71 genomic RNA (1.8 puncta per cell), whereas we detected EV71 capsid on the cell surface. This result suggests that EV71 genomic RNA inside the capsid cannot be

detected by our method. At 10 m.a.i., we detected EV71 capsid, but we observed only 2.7 puncta of EV71 genomic RNA per cell, indicating that EV71 was not uncoated efficiently at this time point. At 20 m.a.i., we observed 8.2 puncta of EV71 genomic RNA per cell, whilst at 30 m.a.i., 40.6 puncta of EV71 genomic RNA per cell were observed. The amount of EV71 genomic RNA significantly increased around five times at 30 m.a.i. compared to that at 20 m.a.i. Furthermore, EV71 RNA and capsid double-labelled vesicles, and EV71 RNA abutting capsid-positive structures underwent clustering at 30 m.a.i, suggesting that uncoating of EV71 robustly occurs at this time point (n = 2 independent experiments).

To confirm whether acidification is required for uncoating, cells were treated with NH_4Cl, which blocks acidification of the lumen of endocytic organelles, and the presence of EV71 genomic RNA was then assessed. RD-hSCARB2 cells were pretreated with or without 40 mM NH_4Cl for 30 minutes followed by addition of EV71 at an MOI of 25. As shown in Fig. 1C, we observed only 1.8 puncta of EV71 genomic RNA per cell even at 30 m.a.i. upon incubation with NH_4Cl, demonstrating that an acidic pH is absolutely required for EV71 uncoating. These experiments were repeated three times. Our results confirm previous finding that EV71 uncoating is triggered by low pH (Yamayoshi et al., 2013, Chen et al., 2012), and suggest that this immunofluorescence approach is a reliable approach for the detection of viral uncoating.

EV71 localizes to LEs during uncoating

It has been hypothesized that EV71 requires hSCARB2 for its uncoating (Yamayoshi et al., 2013). To begin with, we examined whether EV71 traffics with hSCARB2 during the uncoating period using immunofluorescence (Fig. 2). RD-hSCARB2 cells were infected with EV71 at an MOI of 25, and fixed at 5, 10, 20, 30, and 40 m.a.i. followed by immunofluorescence. We detected 129, 111, 102, 123, and 102 EV71-positive puncta at 5, 10, 20, 30, and 40 m.a.i., respectively. As shown

in Fig. 2A and 2E (Fig. 2A for 40 m.a.i.; immunofluorescence at 5, 10, 20, 30 m.a.i. not shown; Fig. 2E, co-localization kinetics), EV71 displays a high level of co-localization with hSCARB2 ranging from 20 to 30% until 40 m.a.i., suggesting that EV71 is sorted together with hSCARB2 in the uncoating period. Next, we examined the intracellular localization of EV71 during this period. As stated in the Materials and Methods, anti-early endosome antigen 1 (EEA1) antibodies were used to identify early endosomes (EE), an anti-CI-M6PR/IGF2R antibody was used for LEs and anti-LAMP1 antibodies were used as lysosome marker. We analyzed a large number of EV71-positive puncta: 60, 92, and 81 at 5 m.a.i., 102, 112, and 100 at 10 m.a.i., 121, 112, and 93 at 20 m.a.i., 103, 101, and 101 at 30 m.a.i., 100, 101, and 103 at 40 m.a.i., for EEA1, CI-M6PR, and LAMP1, respectively. Interestingly, EV71 were found to co-localize with CI-M6PR in around 20% of the EV71-positive organelles from 10 to 30 m.a.i. (Fig. 2C for 30 m.a.i.; immunofluorescence data at 5, 10, 20, 40 m.a.i. not shown; Fig. 2E, co-localization kinetics), whereas only 10% of EV71 co-localized with EEA1 or LAMP1 puncta at this time point (Fig. 2B and 2D for 30 m.a.i.; immunofluorescence at 5, 10, 20, 40 m.a.i. not shown; Fig. 2E, co-localization kinetics; n=3 independent experiments). We confirmed that all EV71 puncta positive for the above markers also co-localize with hSCARB2.

As a control, we checked the intracellular localization of epidermal growth factor (EGF), which is known to traffic to LAMP1-positive LE/lysosomes 30 minutes after internalization (Fig. 3) (Chin et al., 2020). As expected, EGF co-localized with LAMP1 in 48.5% of the organelles, whereas it co-distributes with CI-M6PR only in 24.0% of the puncta (50 EGF + CI-M6PR double-labelled vesicles in 253 EGF-positive puncta; 123 EGF + LAMP1 double-labelled vesicles in 261 EGF-positive puncta; 9 EGF + SCARB2 double-labelled vesicles in 117 EGF-positive puncta). These results suggest that EGF is targeted to lysosomes 30 minutes after internalization in our experimental conditions (n=2 independent experiments).

To confirm EV71 localization during uncoating, we tested the co-distribution of EV71 with the endosomal markers RAB5, RAB7, and RAB9. RAB5 mainly localizes on early endosomes, whereas RAB7 and RAB9 localizes on specific sub-classes of LEs. RD-hSCARB2 cells were infected with EV71 at an MOI of 25, and fixed at 5, 10, 20, 30, and 40 m.a.i. followed by immunofluorescence. We analyzed the following number of EV71-positive puncta; 153, 135, and 128 at 5 m.a.i., 182, 143, and 150 at 10 m.a.i., 145, 154, and 137 at 20 m.a.i., 133, 174, and 150 at 30 m.a.i., 35, 117, and 102 at 40 m.a.i. for RAB5, RAB7, and RAB9, respectively. EV71 shows an extensively colocalization with RAB9 from 10 m.a.i. in over 20% of the organelles (Fig. 4C and 4D), whereas the co-distribution with RAB5 or RAB7 occurs in less than 20% of the cases during this period (Fig. 4A, 4B, and 4D; data at 5, 10, 20, 40 m.a.i. are not shown; n=3 independent experiments). These results indicate that EV71 enters RAB9-positive LE during the uncoating period.

The data shown in Fig. 2 suggest that EV71 is not targeted to LAMP1-positive endolysosomes. Since it has been reported that hSCARB2 co-localized with LAMP2 (Reczek et al., 2007), EV71 may be targeted to LAMP2-positive organelles during uncoating. To investigate whether this is the case, RD-hSCARB2 cells were infected with EV71 at an MOI of 25, and fixed at 30 and 40 m.a.i., followed by immunofluorescence (Fig. S1A and C). Around 20% of EV71 were found to co-localize with LAMP2 at 30 m.a.i., whereas the co-localization decreases around 5% at 40 m.a.i. The experiments were repeated three times and the same trend was observed. These results suggest that the organelles containing EV71 are positive for LAMP2 at 30 m.a.i., but LAMP2 is sorted away before 40 m.a.i. Altogether, our findings demonstrate that EV71 is targeted to endocytic organelles containing LAMP2, RAB9, and CI-M6PR at 30 m.a.i. prior to uncoating.

Uncoating of EV71 does not require LAMP2

It has been previously reported that a specific pool of autophagosomes contains LAMP2,

199 RAB9, and M6PR (Nishida et al., 2009) and that 3-methyladenine (3-MA), which inhibits formation
200 of amphisomes (Nishida et al., 2009, Juenemann and Reits, 2012, Sun et al., 2015), halts immature
201 LEs to gain LAMP2. To examine whether blocking autophagy affects the co-localization of EV71
202 with LAMP2, RAB9, and M6PR at 30 and 40 m.a.i., cells were treated with 3-MA and organelles
203 containing EV71 were analyzed by immunofluorescence and quantified (Fig. S1B and C). RD-
204 hSCARB2 cells were pretreated with or without 5 mM 3-MA for 30 minutes followed by addition of
205 EV71 at an MOI of 25. We analyzed the following numbers of EV71-positive puncta; 106, 130, and
206 140 at 30 m.a.i. without 3-MA, 129, 120, and 202 at 30 m.a.i. with 3-MA, 132, 181, and 125 at 40
207 m.a.i. without 3-MA, 103, 145, and 109 at 40 m.a.i. with 3-MA, for LAMP2, RAB9, and CI-M6PR,
208 respectively. In the presence of 3-MA, EV71 was not targeted to an intracellular compartment
209 positive for LAMP2 even at 40 m.a.i. Interestingly, 3-MA did not affect the ability of EV71 to reach
210 organelles containing RAB9 or CI-M6PR at 30 and 40 m.a.i. The experiments were repeated three
211 times with similar results. These findings suggest that 3-MA blocks the targeting of EV71 to
212 LAMP2-positive organelles, yet does not alter its co-localization with RAB9 or CI-M6PR.
213 To investigate whether LAMP2 is necessary for EV71 uncoating, the effect of 3-MA on light-
214 sensitive EV71 was examined (Fig. S2A). RD-hSCARB2 cells were infected with light-sensitive
215 EV71 at an MOI of 0.004 in the presence or absence of 5 mM 3-MA. Cells were either kept in the
216 dark or irradiated at 450 nm at 10 or 40 m.a.i. to inactivate the intact virus. After irradiation, in
217 selected samples, 3-MA-containing medium was replaced with fresh medium to assess the inhibitory
218 effect this compound on viral replication. Twenty-three hours after infection, cells were harvested
219 and the viral titers determined.
220 In the light-treated samples, viral uncoating was blocked by irradiation, hence the effect of
221 viral uncoating on the viral replication was restricted to the pre-irradiation period. When cells were
222 irradiated at 10 m.a.i., the virus titer decreased by around 5 logs compared to cells kept in the dark in

223 the absence of 3-MA, indicating that this genetically-engineered virus was indeed very sensitive to
224 light. First, we investigated the effect of 3-MA on the productive uncoating of the virus. Light
225 irradiation inhibits additional viral uncoating to enable solely observing the productive uncoating
226 before light irradiation. With light irradiation, 3-MA significantly decreased viral titer in 3-MA (+)
227 to (-) and in 3-MA (+) ($P = 0.0118$ and $P = 0.0057$, respectively; unpaired *t*-test) compared to 3-MA
228 (-). These results indicate that 3-MA inhibited viral productive uncoating before light irradiation,
229 although the virus titer decreased only less than one order of magnitude. Next, we investigated the
230 effect of 3-MA on the replication of the virus. Treatment with 3-MA during viral replication after
231 light irradiation (3-MA (+)) reveals the effect of autophagy on the viral replication process. 3-MA
232 did not decrease viral titer in 3-MA (+) compared to 3-MA (+) to (-) ($P > 0.05$ by unpaired *t*-test),
233 suggesting that 3-MA did not have a significant effect on the viral replication after light irradiation.
234 No significant differences were found in samples kept in the dark, indicating the viral uncoating
235 progressed after 40 m.a.i. in absence of illumination. The experiments were repeated three times
236 and similar results were observed. These findings suggest that 3-MA has only a limited effect on
237 EV71 productive uncoating, and that this process does not require transit through LAMP2-positive
238 organelles.

239 To further explore whether EV71 uncoating fully proceed in the presence of 3-MA, we
240 analyzed the influence of 3-MA on viral uncoating by combined in situ hybridization and
241 immunofluorescence (Fig. S2B). RD-hSCARB2 cells were infected with EV71 at an MOI of 25
242 with or without 3-MA, prior to fixing at specific times after infection. At 0 m.a.i., EV71 RNA was
243 not detected, in agreement to the results shown in Fig. 1C, whilst at 30 m.a.i., viral RNA was detected
244 even in the presence of 3-MA. These results confirm that EV71 undergoes uncoating in the presence
245 of 3-MA in a process that does not require LAMP2. To further confirm EV71 undergoes uncoating
246 in LE in the presence of 3-MA, co-localization of EV71 RNA and CI-M6PR was observed (Fig. S2C).

At 20 m.a.i., the numbers of EV71 RNA + CI-M6PR double labelled puncta in the absence or presence of 3-MA were 19 and 18, respectively, and the numbers of EV71 RNA labelled puncta in the absence or presence of 3-MA was 106 and 64, respectively. At 30 m.a.i., the EV71 RNA + CI-M6PR double-labelled puncta in the absence or presence of 3-MA were 15 and 48, respectively, whereas the EV71 RNA-labelled puncta in the absence or presence of 3-MA were 167 and 200. Co-localization rate of EV71 RNA and CI-M6PR was significantly higher in the presence of 3-MA compared to that observed in the absence of the compound at 30 m.a.i. A similar trend was seen at 20 m.a.i.

In summary, these results suggest that EV71 undergoes uncoating in LEs containing CI-M6PR even in the presence of 3-MA, and this inhibitor boosts the rate of EV71 uncoating in LEs containing CI-M6PR.

Uncoating of EV71 occurs in mature LEs containing intraluminal vesicles

EV71 uncoating starts between 20 m.a.i., when uncoating is negligible, and 30 m.a.i., a time-point in which robust uncoating is observed, yet we lack key information on the nature of these organelles. To further investigate the intracellular trafficking of EV71, we performed transmission electron microscopy (TEM). RD-hSCARB2 cells were infected with purified EV71 at an MOI of 25, fixed at 20 and 30 m.a.i., and then analyzed by TEM (Fig. 5A). At 20 m.a.i., viral particles were surrounded by a single membrane bilayer in organelles resembling Les, but lacking intraluminal vesicles (ILVs). At 30 m.a.i., the viral particles reach LEs containing in some instances ILVs (n=3). These results imply that EV71 is present in the lumen of LEs during its uncoating.

To confirm this conclusion, samples were examined by immunoelectron microscopy (Fig. 5B). At both 20 and 30 m.a.i., gold particles labelling EV71 were found in the lumen of single membrane organelles, likely to be LEs. At 30 m.a.i., gold particles accumulated in single membrane organelles containing ILVs. These results suggest that EV71 accumulates in LE at 20 and 30 m.a.i.

and that during the uncoating period (30 m.a.i.), EV71 specifically localizes at LEs containing ILVs.

It has been reported that ILVs accumulate in LEs following maturation of this endosomal compartment (Nour and Modis, 2014). ILVs in mature LEs are enriched in M6PRs and bis(monoacylglycero)phosphate (BMP) (Nour and Modis, 2014). Based on these considerations, it is plausible that the organelles containing EV71 at 20 m.a.i. are immature LEs, which undergo maturation at 30 m.a.i. acquiring ILVs enriched in BMP. To examine whether the BMP content differs between the vesicles containing EV71 at 20 m.a.i. and those at 30 m.a.i., RD-hSCARB2 cells were infected with EV71 at an MOI of 25, fixed at 20 and 30 m.a.i. and analyzed by immunofluorescence (Fig. 6). We analyzed the following numbers of EV71-positive puncta: 204, 13, 35 at 20 m.a.i. and 317, 83 at 30 m.a.i.; EV71 + BMP double-labelled puncta were 19, 1, 1 at 20 m.a.i. and 144, 34 at 30 m.a.i., respectively. At 20 m.a.i., 6.6% of EV71 co-localized with BMP, whereas the percentage of EV71 co-localized with BMP increased to 43.1% at 30 m.a.i. (n=2 independent experiments), suggesting that LE maturation is important for efficient uncoating of the virus.

CD-M6PR is required for EV71 replication

To investigate whether RABs or M6PRs are essential for EV71 trafficking and replication, we analyzed viral replication in cells in which specific components of the endocytic pathway were downregulated by siRNA. RD cells targeted by siRNA knockdown were infected with EV71-GFP at an MOI of 0.5, fixed after 31 hours from infection prior to fluorescent imaging to assess the percentage of GFP-positive cells in the culture. Protein expression levels in RD cells treated with siRNA were examined by western blotting (Fig. 7A). As shown in Fig. 7B, CD-M6PR siRNA knockdown showed significant inhibition of EV71 replication compared to cells treated with control siRNA ($P = 0.049$), whereas RABs or clathrin heavy chain downregulation did not have any effect

295 (n=3 independent experiments). These results suggest that RAB5, RAB7, and RAB9 are not
296 essential for EV71 replication, whereas CD-M6PR is required for this process, including virus
297 uncoating.
298

Discussion

Although EV71 co-localized with LAMP2, RAB9, and M6PR during its uncoating period, our results suggest that LAMP2 and RAB9 are not essential for EV71 replication. Based on these findings, amphisomes containing LAMP2, RAB9, and M6PR are not likely to be required for EV71 uncoating. Indeed, we could not find EV71 in organelles having double limiting membranes similar to those described for autophagosomes or amphisomes. Thus, EV71 is likely to localize to LEs, and not to amphisomes during the uncoating period (30 to 40 m.a.i.). At 40 m.a.i., it was difficult to detect virus particles by immunoelectron microscopy. Accordingly, the number of viral antigens observed by immunofluorescence was highly reduced at 40 m.a.i. compared to that at 30 m.a.i. or earlier timepoints (data not shown). From these results, the compartments containing EV71 are predicted to undergo fusion with degradative organelles before or at 40 m.a.i. Indeed, RAB9-positive organelles have been reported to fuse with compartments containing RAB7 (Stenmark, 2009), a process that might lead to the degradation of EV71 present in their lumen. (Kirkegaard, 2013). Furthermore, since hSCARB2 and LAMP2 target their binding proteins to lysosomal degradation (Blanz et al., 2010, Reczek et al., 2007, Cuervo and Dice, 1996, Ebato et al., 2008), it is likely that both hSCARB2 and LAMP2 direct EV71 to the degradative pathway. This may explain why we observe an apparent increase of EV71 RNA upon treatment with 3-MA, when organelles containing EV71 does not acquire LAMP2 (Fig. S2C). In the presence of 3-MA, 24% of the viral RNA co-localized with M6PR, in stark contrast to the 9.0% observed in the absence of 3-MA at 30 m.a.i. However, we cannot rule out the possibility that overexpression of hSCARB2 may affect the dynamics of the virus in these cells and as such, influence some of our findings.

Since EV71 starts replication in the cytoplasm by IRES-mediated initiation of translation (Thompson and Sarnow, 2003), it is likely that the entry of genomic viral RNA in the cytoplasm

323 leads to productive infection. On the other hand, the viral RNA present in the lumen of LEs would
324 be exposed to a degradative environment, leading to abortive infection (Fig. S1). In the case the
325 uncoating of the virus occurs on ILVs in LEs, viral RNA is released into LE lumen, whereas when
326 the uncoating occurs on LE membrane, viral RNA is released into cytoplasm (Dang et al., 2014).
327 As shown in Fig. S2C, we observed more EV71 RNA in the presence of 3-MA than in the absence
328 of 3-MA, whereas 3-MA inhibited virus productive uncoating (Fig. S2A). These results suggest
329 that some of the EV71 uncoating occur on ILVs in LEs and 3-MA inhibits uncoated EV71 RNA to
330 leave LEs at 30 m.a.i. Thus, it is likely that 3-MA increases abortive infection of EV71.
331 According to a previous report (Lee et al., 2014), 3-MA reduced the replication and pathogenesis of
332 EV71 (strain 4643) in a suckling mouse model. In 16HBE cells, 10 mM 3-MA inhibited the
333 replication of EV71 (sub-genotype C4, GenBank: EU812515.1) (Song et al., 2018). Our strategy
334 utilizing RD-hSCARB2 cells and light sensitive virus allowed us to analyze viral uncoating and
335 replication separately. As a result, we found that 5 mM 3-MA did not affect the productive
336 uncoating of EV71 and did not have a significant effect on viral replication (Fig. S2A).
337 The pH of the immature LEs is around pH 6.0, whereas mature LEs enriched in BMP-
338 containing ILVs is pH 5.5 or lower (Nour and Modis, 2014). EV71 bound to hSCARB2
339 significantly starts uncoating at pH 6.0 or below in vitro (Yamayoshi et al., 2013). At pH 6.5,
340 2.6% of the virus was uncoated after 1 h, whereas this percentage raises to 5.0% and 6.1% at pH 6.0
341 or pH 5.5, respectively. From these results, only cellular compartments with a pH of 6.0 or lower
342 would be compatible with viral uncoating. However, in the case of poliovirus (PV), which
343 requires solely its receptor for uncoating, about 90% of the virus particles lose their coat 1 hour
344 after addition of its receptor (Arita et al., 1998). Thus, the efficiency for uncoating of EV71 bound
345 to hSCARB2 at pH 6.0 is likely to be much lower than that of PV. This difference might imply
346 that other factors assist EV71 uncoating besides hSCARB2 and the low pH.

Our results suggest that CD-M6PR is essential for EV71 replication, including uncoating. CD-M6PR is enriched in ILVs (Dikic, 2006). Both CI-M6PR and CD-M6PR have M6P-binding sites, and CI-M6PR interacts with hSCARB2 holding β-GC via M6P in cis (Zhao et al., 2014). Since CD-M6PR has a short extracellular domain and hSCARB2 is modified with M6P at the distal site from the membrane, CD-M6PR might interact with M6P on hSCARB2 in trans. The hypothesized interaction between CD-M6PR and hSCARB2 in trans would facilitate the binding between EV71 with another hSCARB2 molecule. It is possible that the action of multiple hSCARB2 molecules localized on both LEs and the ILVs would enhance the uncoating kinetics of EV71. However, future work will be necessary to validate this hypothesis. Since knockdown of M6PR may influence the distribution of SCARB2, we cannot exclude the possibility that M6PR interferes indirectly with the uncoating of the virus.

Efficient uncoating of EV71 occurs at mature LEs containing ILVs. Both immature and mature LEs have a pH low enough for EV71 uncoating; however, EV71 is not uncoated efficiently in immature LEs. A possible reason for this might reside in the structural difference between immature and mature LEs. In immature LEs, which harbour fewer ILVs, EV71 would be mainly localized mainly on the delimiting LE membrane, since uncoating of the virus occurs solely on membranes. In contrast, in mature LEs, both EV71 and hSCARB2 would localize on LE and ILV membranes, thus increasing the potential for uncoating. An alternative, yet not exclusive possibility is linked to the pH dependent interaction of hSCARB2 with β-GC. Previous in vitro studies demonstrated that hSCARB2 binds β-GC at pH 6.5, whereas it does not at pH 5.5 (Zhao et al., 2014). Interestingly, the binding site(s) of hSCARB2 for β-GC (amino acids 145-222 (Zachos et al., 2012) or 150–167 (Reczek et al., 2007)) overlaps with the binding site(s) for EV71 (amino acids 142-204 (Yamayoshi and Koike, 2011) or 144–151 (Chen et al., 2012)), and exogenous β-GC has been found to interfere with EV71 binding to hSCARB2 on the cell surface (Nakata et al.,

371 2017). This implies that release of β-GC from hSCARB2 at pH 5.5 may enhance the interaction

372 between EV71 and hSCARB2, thus boosting EV71 uncoating.

373

Materials and Methods

Cells

RD cells and Vero cells were cultured in Dulbecco's modified Eagle's medium (Nissui) supplemented with 5% fetal bovine serum (FBS) and penicillin-streptomycin (Life Technologies) (5% FBS-DMEM). RD-hSCARB2 cells (generously gifted by Dr. K. Fujii) were cultured in 5% FBS-DMEM supplemented with 4 μg/ml puromycin (Calbiochem). Cells had been tested for contamination and mycoplasma infection.

Viruses

The EV71 strains SK-EV006/Malaysia/97 (SK-EV006; genogroup B) (Shimizu et al., 1999), EV71/86-11316 NETH-86 (genogroup B) (Nakajima et al., 2012) and EV71-GFP (generously gifted by Dr. M. Arita), which expresses GFP upon viral replication (Yamayoshi et al., 2013), were used in this study. EV71/86-11316 NETH-86 was used for producing light-sensitive virus, and EV71-GFP was used in siRNA knockdown experiment. Unless otherwise stated, we used purified EV71 SK-EV006 as a representative strain of EV71. Experiments using recombinant DNA and pathogens were approved by the Committee for Experiments using Recombinant DNA and Pathogens at the Tokyo Metropolitan Institute of Medical Science (TMiMS).

Antibodies

We used the following primary antibodies for immunofluorescence and western blotting: anti-SCARB2 goat antibodies (1:1250, AF1966, R&D Systems), anti-EEA1 rabbit antibodies (1:500, ab2900, Abcam), anti-clathrin heavy chain rabbit antibodies (1:1,000, ab21679, Abcam), anti-RAB5 rabbit antibodies (1:1,000, ab18211, Abcam), anti-RAB7 rabbit monoclonal antibody [EPR7589] (1:250 for immunofluorescence, 1:1,000 for western blotting, ab137029, Abcam), anti-RAb9 mouse monoclonal antibody [EPR13272] (1:100 for immunofluorescence, 1:1,000 for western blotting,

ab179815, Abcam), anti-LAMP1 rabbit antibodies (1:1,000, ab24170, Abcam), purified anti-LBPA mouse antibody (6C4) for BMP staining (1:500, Z-PLBPA, Echelon), anti-LAMP2 [EPR13272] rabbit monoclonal antibody (1:100, ab37024, Abcam), anti-EV71 mouse monoclonal antibody N3 (1:9000, from G. Liu and P. C. Choi-Sing), anti-EV71 serum (1:1,000 for immunofluorescence, 1:200 for immunoelectron microscopy, kindly provided by H. Shimizu, NIID, Japan) (Nagata et al., 2002), anti-β-actin AC74 monoclonal antibody (1:5,000, A5316, Sigma-Aldrich). For anti-M6PR antibodies, we used anti-CI-M6PR/IGF2R rabbit monoclonal antibody [EPR6599] (1:250, ab124767, Abcam), anti-CD-M6PR rabbit polyclonal antibodies (1:50, ABIN357957, Antibodies-online) and chicken polyclonal antibodies (1:200, GW21444, Sigma) for immunofluorescence, and anti-CI-M6PR/IGF2R rabbit antibody [EPR6599] (1:50,000, ab124767, Abcam), anti-CD-M6PR chicken polyclonal antibodies (1:500, GW21444, Sigma) for western blotting. As secondary antibodies, we used AlexaFluor488, 568, and 647 donkey, or goat anti-mouse, rabbit, chicken or goat IgG (H+L) (1:1,000, Life Technologies), anti-IgG (H+L), 5 nm gold-conjugated goat anti-rabbit IgG (H+L), EM (1:100, EM.GARHL5, BBI Solutions), anti-rabbit IgG HRP, and anti-mouse IgG HRP (1:100,000, Jackson Immunoresearch).

Virus purification

RD-hSCARB2 cells were infected with EV71 SK-EV006/Malaysia/97 strain at an MOI of 5. Cells and media were frozen 18 hours post-infection. After thawing, cell debris was removed by centrifugation in a NA-4HS rotor (TOMY) at 10,000 rpm for 20 minutes at 4°C. The supernatant was layered onto a 1.25 g/ml and 1.48 g/ml CsCl discontinuous step gradient in phosphate-buffered saline [PBS (-)] (per liter, 8.00 g NaCl, 1.15 g Na_2HPO_4, 0.20 g KCl, 0.20 g KH_2PO_4 [pH 7.4]). Native virions (F-particles) were collected from a fraction between the 1.25 g/ml and 1.48 g/ml CsCl. The F-particles were applied onto PD-10 or NAP5 column and eluted with PBS (-). After fractionation (0.2 ml/fraction), the fractions that included the F-particles were collected.

Light-sensitive EV71

The experiments were performed in the dark unless stated otherwise. RD-hSCARB2 cells were infected with EV71/86-11316 NETH-86 strain at an MOI of 0.1 in 10 ml of 5% FBS-DMEM and incubated at 37°C for 1 hour. Upon removal of the supernatant, cells were washed with DMEM and then 20 ml of 5% FBS-DMEM and 40 μg/ml neutral red were added. Around 24 hours after infection, the infected cells were transferred at -80°C followed by freezing and thawing three times. After a sonication for 30 minutes on ice, the virus solution was centrifuged and the supernatant was recovered followed by titration in the dark or after light irradiation using $TCID_{50}$ in VERO cells. RD-hSCARB2 was infected with the recovered virus similarly to the first stage infection. The virus supernatant was recovered followed by titration using $TCID_{50}$ in VERO cells and used for experiments. For light irradiation of the light-sensitive virus, light was shone 30 cm apart from the plates by Grassy LeDio RS122 Fresh White LED light (Volxjapan) including 450 nm spectrum peak for 30 minutes at room temperature. The temperature of the plates was strictly monitored to avoid cell overheating. In experiments described in Fig. 1A and 1B, RD-hSCARB2 cells were infected with light-sensitive EV71 at a MOI of 10 and cells were either kept in the dark or irradiated at the indicated time after infection to inactivate intact virus. Experiments were performed in triplicate. Seven hours after infection, cells were harvested and the viral titers were determined using $TCID_{50}$ in VERO cells. In the experiments shown Fig. S2A, RD-hSCARB2 cells were infected with light-sensitive EV71 at an MOI of 0.004 in the presence or absence of 5 mM 3-MA. Cells were either kept in the dark or irradiated with light to inactivate the intact virus at 10 or 40 m.a.i. After irradiation, the medium containing 3-MA was replaced with fresh medium in selected samples to assess the inhibitory effect of 3-MA on viral replication. These experiments were performed in triplicate. Twenty-three hours after infection, cells were harvested and the viral titers determined using $TCID_{50}$ in VERO cells.

Immunofluorescence

RD-SCARB2 cells and RD cells were seeded onto 16-well Lab-Tek Chamber Slide (Nunc). One day after seeding, purified EV71 were added at an MOI of 25 at 4°C to allow viral attachment to the cell surface without entry. In selected cases, cells were pretreated with or without 40 mM NH_4Cl or 5 mM 3-MA for 30 minutes. Cells were then shifted to 37°C (designated as time 0), washed with PBS (-) with or without NH_4Cl or 3-MA, fixed in PBS containing 4% paraformaldehyde (PFA) for 15 minutes and washed four times with cold PBS before further processing. In Fig. 3, to detect EGF localization, we added 2 μg/ml of biotinylated EGF bound to AlexaFluor555 streptavidin (Invitrogen) in the medium. Fixed cells were incubated with PBS containing 0.05% saponin and 5% bovine serum albumin fraction V (Sigma) to permeabilize the membrane and block nonspecific reactions. Samples were incubated overnight at 4°C with primary antibodies. After being washed with PBS (-), samples were then incubated with the secondary antibodies for 90 minutes at room temperature, and after another PBS (-) wash, mounted in Vectashield with DAPI Mounting Medium (Vector Laboratories). Samples were imaged with a laser-scanning microscope (TCS SP2, Leica Microsystems). Images were analyzed by Imaris (Zeiss).

In situ immunofluorescence analysis

Cells were pretreated with or without 40 mM NH_4Cl or 5 mM 3-MA for 30 minutes followed by addition of purified EV71 at an MOI of 25 with or without NH_4Cl or 3-MA. Infected cells were washed twice with PBS (-) with or without NH_4Cl or 3-MA followed by fixation with 4% PFA at room temperature for 30 minutes. Fixed cells were washed with PBS (-) 3 times, dehydrated with ethanol and transferred at -20°C. After rehydration, samples were treated with proteases and in situ hybridization was performed using QuantiGene ViewRNA ISH (Thermo Fisher) according to manufacturer's instructions followed by fluorescence analysis. EV71 sequence was from nucleotide number 3008 to 3609 of SK-EV006/Malaysia/97 strain (GenBank: AB469182.1) (Shimizu et al.,

1999).

EV71 infection in knockdown cells

RD cells were seeded in 8 well culture slides (BD Falcon) one day before transfection with siRNAs. siRNAs, pre-designed or validated *Silencer* Select siRNAs were obtained from Life Technologies. As a negative control, *Silencer* Negative Control No. 1 siRNA (Life Technologies) was used. Transfection of siRNAs into RD cells was performed using Lipofectamine 3000 (Invitrogen, Carlsbad, CA), which was diluted in Opti-MEM and added to siRNA diluted in Opti-MEM. After an incubation of 5 minutes at room temperature, the mixture was added to cells and incubated at 37°C for 4 hours followed by medium exchange. Two days later, cells were infected with EV71-GFP at an MOI of 0.5. Experiment were performed in triplicate for knockdown samples and sextuplicate for siControl. In parallel, cells in other wells were fixed in PBS (-) containing 4% PFA for 30 minutes followed by immunostaining of target proteins to check the knockdown efficiency. Immunostaining showed knockdown efficiency consistent with the results obtaining using western blotting. After 24 hours incubation at 37°C, infected cells were fixed in PBS containing 4% PFA for 30 minutes and washed four times with PBS. The numbers of GFP-positive cells were counted and the ratio against the numbers of DAPI-positive cells was analyzed. GFP positive cells were observed by VS120 Virtual Slide Microscope (Olympus) and analyzed using Image J software (National Institutes of Health, USA). To analyze protein expression by immunofluorescence, cells were stained as described above and imaged with a laser-scanning microscope. To quantify protein expression, samples were loaded onto 12% Mini-Protean TGX precast gels (Bio-Rad), followed by western blotting with anti-RAB5, RAB7, RAB9, M6PRs, and clathrin heavy chain antibodies. RD cells treated with siRNAs were detached with 0.02% EDTA-PBS and dissolved in 100 µl of electrophoresis sample buffer (50 mM Tris-HCl, pH 6.8, 10% glycerol, 2% sodium dodecyl sulfate, 0.1% bromophenol blue in H_2O) per 2×10^5 cells, followed by sonication and addition of 5% v/v of

2-mercaptoethanol. Samples were loaded onto precast gels mini-Protein TGX Gels 12% (BioRad), followed by western blotting. Band intensities were analyzed using Image J.

Electron microscopy

For transmission electron microscopy, cells washed with PBS (-) were fixed in 2% (w/v) PFA and 2.5% (v/v) glutaraldehyde in PBS (-) for 2.5 h. After osmication in 1% (w/v) osmium tetroxide, specimens were dehydrated through a graded alcohol series, and embedded in Epon 812 (TAAB Laboratories). Ultrathin sections were cut on an Ultracut microtome (Leica EM-UC6) and stained with uranyl acetate and lead citrate. Sections were observed under a transmission electron microscope (Hitachi H-7650).

For immuno-electron microscopy, cells washed with PBS (-) were fixed in 4% PFA and 0.05% glutaraldehyde in PBS (-) for 2.5 h. The immunogold labeling followed the method of Akagi *et al.* (Akagi et al., 2006), except for the antibodies. After blocking with 10% normal goat serum, sections were incubated in Tris-buffered saline (TBS) containing antibody against EV71 for 24–48 hours at 4°C and then washed with TBS and incubated with gold particle-conjugated secondary antibodies for 2 hours at room temperature. Thereafter, the sections were rinsed and embedded with a mixture of 1% polyvinyl alcohol containing 0.1% uranyl acetate, dried, and observed with an electron microscope (Hitachi H-7650).

Statistical analysis

Statistical analysis was done using GraphPad Prism 7.00 (GraphPad Software Inc.). A two-tailed unpaired *t*-test has been performed in Figs. 1D, 3B, S2A, 6B and 7B, and a two-tailed Fisher's exact test has been performed in Figs. S1C and S2C.

Acknowledgements

We thank Dr. S. Koike (TMiMS) for the primary project assignment for S.O., allowing S.O. to be a member of the laboratory, allowing S.O. to use facilities and the laboratory area, and generously host S.O. instruments and samples. We thank Dr. K. Fujii (TMiMS) for generously gifting RD-hSCARB2 cells, and Dr. H. Shimizu and Dr. M. Arita (National Institute of Infectious Diseases, Japan) for kindly providing the virus strains and GFP-EV71 plasmid, respectively. We appreciate Prof. K.T. Wong giving an opportunity for S.H.T. to engage in research with S.O. and Dr. K. Ikeda (TMiMS) for generously allowing to prepare and publish this manuscript.

Competing interests

The authors declare no competing or financial interests.

Author contributions

S.O. was involved in project planning. S.O., S.H.T. and K.I. were involved in experimental work and data analysis. E.I., K.O., K. Hagiwara and T.H. performed the experiments. C.L. and P.C.C. provided the monoclonal antibody against EV71. K. Hanaki. and G.S. were involved in data analysis. S.O. wrote the manuscript, which was revised by G.S., P.C.C., K. Hanaki and S.O.

Funding

This work was supported in part by project research funding for Neurovirology Project from TMiMS, a Grant-in-aid for Scientific Research (C) (25460583) from the Japan Society for the Promotion of Science (S.O.), and in part by The Naito Foundation Subsidy for Female Researchers after Maternity Leave (S.O.). S.H.T. was supported by High Impact Research UM.C/625/1/HIR/MOHE/MED/06 (UM.0000064/HIR.C1) from the Ministry of Higher Education, Malaysia government. G.S. is supported by Wellcome Senior Investigator Awards (107116/Z/15/Z and 223022/Z/21/Z), and a UK Dementia Research Institute Foundation award (UKDRI-1005).

548 **References**

549

550 **Akagi, T., Ishida, K., Hanasaka, T., Hayashi, S., Watanabe, M., Hashikawa, T. & Tohyama, K.**
551 (2006). Improved methods for ultracryotomy of CNS tissue for ultrastructural and
552 immunogold analyses. *J Neurosci Methods,* **153,** 276-282.

553 **Arita, M., Koike, S., Aoki, J., Horie, H. & Nomoto, A.** (1998). Interaction of poliovirus with its
554 purified receptor and conformational alteration in the virion. *J Virol,* **72,** 3578-3586.

555 **Blanz, J., Groth, J., Zachos, C., Wehling, C., Saftig, P. & Schwake, M.** (2010). Disease-causing
556 mutations within the lysosomal integral membrane protein type 2 (LIMP-2) reveal the nature
557 of binding to its ligand beta-glucocerebrosidase. *Hum Mol Genet,* **19,** 563-572.

558 **Blomberg, J., Lycke, E., Ahlfors, K., Johnsson, T., Wolontis, S. & Von Zeipel, G.** (1974). Letter:
559 New enterovirus type associated with epidemic of aseptic meningitis and-or hand, foot, and
560 mouth disease. *Lancet,* **2,** 112.

561 **Chen, P., Song, Z., Qi, Y., Feng, X., Xu, N., Sun, Y., Wu, X., Yao, X., Mao, Q., Li, X., Dong, W.,**
562 **Wan, X., Huang, N., Shen, X., Liang, Z. & Li, W.** (2012). Molecular determinants of
563 enterovirus 71 viral entry: cleft around GLN-172 on VP1 protein interacts with variable region
564 on scavenge receptor B 2. *J Biol Chem,* **287,** 6406-6420.

565 **Chin, T. M., Boopathy, G. T. K., Man, E. P. S., Clohessy, J. G., Csizmadia, E., Quinlan, M. P.,**
566 **Putti, T., Wan, S. C., Xie, C., Ali, A., Wai, F. C., Ong, Y. S., Goh, B. C., Settleman, J.,**
567 **Hong, W., Levantini, E. & Tenen, D. G.** (2020). Targeting microtubules sensitizes drug
568 resistant lung cancer cells to lysosomal pathway inhibitors. *Theranostics,* **10,** 2727-2743.

569 **Cuervo, A. M. & Dice, J. F.** (1996). A receptor for the selective uptake and degradation of proteins
570 by lysosomes. *Science,* **273,** 501-503.

571 **Dang, M., Wang, X., Wang, Q., Wang, Y., Lin, J., Sun, Y., Li, X., Zhang, L., Lou, Z., Wang, J.**

572 **& Rao, Z.** (2014). Molecular mechanism of SCARB2-mediated attachment and uncoating of
573 EV71. *Protein Cell,* **5,** 692-703.
574 Dikic, I. (ed.) 2006. *Sorting to the Biosynthetic Pathway*: Springer.
575 **Ebato, C., Uchida, T., Arakawa, M., Komatsu, M., Ueno, T., Komiya, K., Azuma, K., Hirose, T.,**
576 **Tanaka, K., Kominami, E., Kawamori, R., Fujitani, Y. & Watada, H.** (2008). Autophagy
577 is important in islet homeostasis and compensatory increase of beta cell mass in response to
578 high-fat diet. *Cell Metab,* **8,** 325-332.
579 **Eskelinen, E. L.** (2006). Roles of LAMP-1 and LAMP-2 in lysosome biogenesis and autophagy. *Mol*
580 *Aspects Med,* **27,** 495-502.
581 **Eskelinen, E. L., Tanaka, Y. & Saftig, P.** (2003). At the acidic edge: emerging functions for
582 lysosomal membrane proteins. *Trends Cell Biol,* **13,** 137-145.
583 **Hagiwara, A., Tagaya, I. & Yoneyama, T.** (1978). Epidemic of hand, foot and mouth disease
584 associated with enterovirus 71 infection. *Intervirology,* **9,** 60-63.
585 **Hussain, K. M., Leong, K. L., Ng, M. M. & Chu, J. J.** (2011). The essential role of clathrin-
586 mediated endocytosis in the infectious entry of human enterovirus 71. *J Biol Chem,* **286,** 309-
587 321.
588 **Juenemann, K. & Reits, E. A.** (2012). Alternative macroautophagic pathways. *Int J Cell Biol,* **2012,**
589 189794.
590 **Kirkegaard, T.** (2013). Emerging therapies and therapeutic concepts for lysosomal storage diseases.
591 *Expert Opinion on Orphan Drugs,* **1,** 385-404.
592 **Lee, Y. R., Wang, P. S., Wang, J. R. & Liu, H. S.** (2014). Enterovirus 71-induced autophagy
593 increases viral replication and pathogenesis in a suckling mouse model. *J Biomed Sci,* **21,** 80.
594 **Lin, Y. W., Lin, H. Y., Tsou, Y. L., Chitra, E., Hsiao, K. N., Shao, H. Y., Liu, C. C., Sia, C., Chong,**
595 **P. & Chow, Y. H.** (2012). Human SCARB2-mediated entry and endocytosis of EV71. *PLoS*

One, **7,** e30507.

Mcminn, P. C. (2002). An overview of the evolution of enterovirus 71 and its clinical and public health significance. *FEMS Microbiol Rev,* **26,** 91-107.

Nagata, N., Shimizu, H., Ami, Y., Tano, Y., Harashima, A., Suzaki, Y., Sato, Y., Miyamura, T., Sata, T. & Iwasaki, T. (2002). Pyramidal and extrapyramidal involvement in experimental infection of cynomolgus monkeys with enterovirus 71. *J Med Virol,* **67,** 207-216.

Nakajima, N., Kitamori, Y., Ohnaka, S., Mitoma, Y., Mizuta, K., Wakita, T., Shimizu, H. & Arita, M. (2012). Development of a transcription-reverse transcription concerted reaction method for specific detection of human enterovirus 71 from clinical specimens. *J Clin Microbiol,* **50,** 1764-1768.

Nakata, K., Takeda, S., Tanaka, A., Kwang, J. & Komano, J. (2017). Antiviral activity of acid beta-glucosidase 1 on enterovirus 71, a causative agent of hand, foot and mouth disease. *J Gen Virol,* **98,** 643-651.

Nishida, Y., Arakawa, S., Fujitani, K., Yamaguchi, H., Mizuta, T., Kanaseki, T., Komatsu, M., Otsu, K., Tsujimoto, Y. & Shimizu, S. (2009). Discovery of Atg5/Atg7-independent alternative macroautophagy. *Nature,* **461,** 654-658.

Nour, A. M. & Modis, Y. (2014). Endosomal vesicles as vehicles for viral genomes. *Trends Cell Biol,* **24,** 449-454.

Pfeffer, S. R. (2017). Rab GTPases: master regulators that establish the secretory and endocytic pathways. *Mol Biol Cell,* **28,** 712-715.

Plevka, P., Perera, R., Cardosa, J., Kuhn, R. J. & Rossmann, M. G. (2012). Crystal structure of human enterovirus 71. *Science,* **336,** 1274.

Racaniello, V. (2007). *Fields Virology, 5th ed.,* Philadelphia, PA, Lippincott Williams & Wilkins.

Reczek, D., Schwake, M., Schroder, J., Hughes, H., Blanz, J., Jin, X., Brondyk, W., Van Patten,

S., Edmunds, T. & Saftig, P. (2007). LIMP-2 is a receptor for lysosomal mannose-6-phosphate-independent targeting of beta-glucocerebrosidase. *Cell,* **131,** 770-783.

Rossmann, M. G. & Johnson, J. E. (1989). Icosahedral RNA virus structure. *Annu Rev Biochem,* **58,** 533-573.

Semerdjieva, S., Shortt, B., Maxwell, E., Singh, S., Fonarev, P., Hansen, J., Schiavo, G., Grant, B. D. & Smythe, E. (2008). Coordinated regulation of AP2 uncoating from clathrin-coated vesicles by rab5 and hRME-6. *J Cell Biol,* **183,** 499-511.

Shimizu, H., Utama, A., Yoshii, K., Yoshida, H., Yoneyama, T., Sinniah, M., Yusof, M. A., Okuno, Y., Okabe, N., Shih, S. R., Chen, H. Y., Wang, G. R., Kao, C. L., Chang, K. S., Miyamura, T. & Hagiwara, A. (1999). Enterovirus 71 from fatal and nonfatal cases of hand, foot and mouth disease epidemics in Malaysia, Japan and Taiwan in 1997-1998. *Jpn J Infect Dis,* **52,** 12-15.

Song, J., Hu, Y., Li, J., Zheng, H., Wang, J., Guo, L., Shi, H. & Liu, L. (2018). Suppression of the toll-like receptor 7-dependent type I interferon production pathway by autophagy resulting from enterovirus 71 and coxsackievirus A16 infections facilitates their replication. *Arch Virol,* **163,** 135-144.

Stenmark, H. (2009). Rab GTPases as coordinators of vesicle traffic. *Nat Rev Mol Cell Biol,* **10,** 513-525.

Sun, N., Yun, J., Liu, J., Malide, D., Liu, C., Rovira, Ii, Holmstrom, K. M., Fergusson, M. M., Yoo, Y. H., Combs, C. A. & Finkel, T. (2015). Measuring In Vivo Mitophagy. *Mol Cell,* **60,** 685-696.

Thompson, S. R. & Sarnow, P. (2003). Enterovirus 71 contains a type I IRES element that functions when eukaryotic initiation factor eIF4G is cleaved. *Virology,* **315,** 259-266.

Vega, M. A., Segui-Real, B., Garcia, J. A., Cales, C., Rodriguez, F., Vanderkerckhove, J. &

644 **Sandoval, I. V.** (1991). Cloning, sequencing, and expression of a cDNA encoding rat LIMP
645 II, a novel 74-kDa lysosomal membrane protein related to the surface adhesion protein CD36.
646 *J Biol Chem,* **266,** 16818-16824.
647 **Wandinger-Ness, A. & Zerial, M.** (2014). Rab proteins and the compartmentalization of the
648 endosomal system. *Cold Spring Harb Perspect Biol,* **6,** a022616.
649 **Wang, X., Peng, W., Ren, J., Hu, Z., Xu, J., Lou, Z., Li, X., Yin, W., Shen, X., Porta, C., Walter,**
650 **T. S., Evans, G., Axford, D., Owen, R., Rowlands, D. J., Wang, J., Stuart, D. I., Fry, E. E.**
651 **& Rao, Z.** (2012). A sensor-adaptor mechanism for enterovirus uncoating from structures of
652 EV71. *Nat Struct Mol Biol,* **19,** 424-429.
653 **Yamayoshi, S. & Koike, S.** (2011). Identification of a human SCARB2 region that is important for
654 enterovirus 71 binding and infection. *J Virol,* **85,** 4937-4946.
655 **Yamayoshi, S., Ohka, S., Fujii, K. & Koike, S.** (2013). Functional comparison of SCARB2 and
656 PSGL1 as receptors for enterovirus 71. *J Virol,* **87,** 3335-3347.
657 **Yamayoshi, S., Yamashita, Y., Li, J., Hanagata, N., Minowa, T., Takemura, T. & Koike, S.** (2009).
658 Scavenger receptor B2 is a cellular receptor for enterovirus 71. *Nat Med,* **15,** 798-801.
659 **Zachos, C., Blanz, J., Saftig, P. & Schwake, M.** (2012). A critical histidine residue within LIMP-2
660 mediates pH sensitive binding to its ligand beta-glucocerebrosidase. *Traffic,* **13,** 1113-1123.
661 **Zhao, Y., Ren, J., Padilla-Parra, S., Fry, E. E. & Stuart, D. I.** (2014). Lysosome sorting of beta-
662 glucocerebrosidase by LIMP-2 is targeted by the mannose 6-phosphate receptor. *Nat Commun,*
663 **5,** 4321.
664
665

Figure legends

Figure 1. EV71 is uncoated at 30 m.a.i. and is dependent on acidification

(A) Experimental protocol for infection of RD-hSCARB2 cells with light-sensitive EV71. The red arrow indicates virus addition, the green arrow indicates the recovery of the infected cells followed by the titration of the live virus, black arrowheads indicate the start of light irradiation, gray areas indicate the periods without the light irradiation, and yellow area indicates the periods with the light irradiation. The time after the infection with light-sensitive virus is indicated. (B) Virus titer of the recovered virus. Horizontal axis indicates the onset of light irradiation after infection. The top line represents the virus titer without irradiation. Error bars represent SD. (C) In situ hybridization for RNA genome of EV71 and immunofluorescence for the capsid proteins after infection of RD-hSCARB2 cells with EV71 in the absence or presence of NH_4Cl. The time of fixation after infection is indicated. DAPI is in blue, EV71 RNA genome is in green, whilst EV71 capsid antigens are in red. The panels on the right are enlarged 3D cross-section views of the dashed rectangles in the merged panels. Arrowheads indicate EV71 RNA + capsid double-labelled clustered vesicles. Insets are 400% enlarged panels of the arrowhead areas. Representative images are shown. Scale bar, 10 μm. (D) The numbers of visible green dots corresponding to EV71 RNA genomes per cell were shown. Number of z stack sets was three except for the 30 min NH_4Cl+ sample (two). **, $P < 0.01$. Statistical significance was determined by a two-tailed, unpaired *t*-test. Error bars represent s.d.

Figure 2. EV71 co-distributes with hSCARB2 and M6PR, but not with LAMP1 until 40 m.a.i.

Co-localization of EV71 and hSCARB2 (A), EEA1 (B), M6PR (C), or LAMP1 is shown by immunofluorescence (D). RD-hSCARB2 cells were infected with EV71 and fixed 30 minutes (B-

690 D) or 40 minutes (A) after infection followed by immunofluorescence. DAPI is in blue, EV71 antigen
691 is in green, whereas hSCARB2 or other markers are in red. The panels on the right are enlarged 3D
692 cross-section views of the dashed rectangles in the merged panels. Arrowheads indicate co-
693 localization of EV71 with markers. Representative images are shown. Scale bars, 10 μm. (E)
694 Kinetics of co-localization of EV71 with hSCARB2 or other markers. Times indicate the time after
695 infection.
696
697 **Figure 3. EGF co-localizes with LAMP1 at 30 m.a.i.**
698 (A) Co-localization of EGF with M6PR, LAMP1 or SCARB2 is shown by immunofluorescence of
699 EGF and M6PR, LAMP1 and SCARB2. RD-hSCARB2 cells were infected with EV71 and then
700 fixed 30 minutes after the addition of EGF followed by immunofluorescence DAPI is in blue, EGF
701 is in green, whereas organelle markers are in red. The panels on the right are enlarged 3D cross-
702 section views of the dashed rectangles in the merged panels. Arrowheads indicate co-localization
703 of EGF with markers. Representative images are shown. Scale bar, 10 μm. (B) Quantification
704 of co-localization of EGF with specific markers. Number of z stack sets was two except SCARB2
705 was three. ns, not significant, **, $P < 0.01$. Statistical significance was determined by a two-tailed,
706 unpaired *t*-test. Error bars represent s.d.
707
708 **Figure 4. EV71 co-distributes with RAB9 during the uncoating period**
709 Co-localization of EV71 with RAB5, RAB7, or RAB9 is shown by immunofluorescence of EV71
710 and RAB5 (A), RAB7 (B), or RAB9 (C). RD-hSCARB2 cells were infected with EV71 and fixed
711 30 minutes after infection, followed by immunofluorescence. DAPI is in blue, EV71 antigen is in
712 green, whereas marker antigens are in red. The panels on the right are enlarged 3D cross-section
713 views of the dashed rectangles in the merged panels. Arrowheads indicate co-localization of EV71

with markers. Representative images are shown. Scale bar, 10 μm. (D) Kinetics of co-localization of EV71 with the different markers. Times indicate the time after infection.

Figure 5. EV71 particles are incorporated into LEs

(A) Transmission electron microscopy. RD-hSCARB2 cells were infected with EV71 and fixed at 20 or 30 m.a.i. Times indicate the time after infection. Arrowheads indicate representative EV71-like particles in LE. (B) Immuno-electron microscopy. Gold particles label EV71 antigen. Arrowheads indicate representative gold particles existed in the lumen of single membrane compartments without ILV at 20 m.a.i., and representative gold particles accumulated in single membrane organelles containing ILVs at 30 m.a.i. The experiments were repeated two times and the same trends were observed. Scale bar, 200 nm.

Figure 6. EV71 translocates into BMP-enriched LE at 30 m.a.i.

(A) RD-hSCARB2 cells were infected with EV71 and then fixed 20 minutes or 30 minutes after the infection followed by immunofluorescence. DAPI is in blue, EV71 antigen is in green, whereas BMP is labelled in red. The panels on the right are enlarged 3D cross-section views of the dashed rectangles in the merged panels. Arrowheads indicate co-localization of EV71 with BMP. Representative images are shown. Scale bar, 10 μm. (B) Co-localization rate of EV71 with BMP at 20 or 30 m.a.i. **, $P < 0.01$. Statistical significance was determined by a two-tailed, unpaired *t*-test. Error bars represent s.d.

Figure 7. CD-M6PR is essential for EV71 replication

(A) Western blotting of RAB5, RAB7, RAB9, CD-M6PR, CI-M6PR and clathrin heavy chain in cells in which these genes have been targeted by siRNA knockdown. The expression of β-actin was

738 examined as loading control. Triangles indicate molecular weight markers. Black dots indicate
739 the predicted molecular weight of the proteins. The numbers are the densities and the ratio of anti-
740 markers/anti β-actin. (B) RD cells were treated with siRNAs targeting RAB5, RAB7, RAB9, CD-
741 M6PR, CI-M6PR or clathrin heavy chain and then infected with EV71-GFP. Cells were fixed at 31
742 hours after infection, followed by fluorescent imaging. GFP-positive cells were counted and their
743 percentage against the total number of DAPI-positive cells plotted. *, $P < 0.05$. Statistical
744 significance was determined by a two-tailed, unpaired *t*-test. Error bars represent s.d.
745

Figure 1

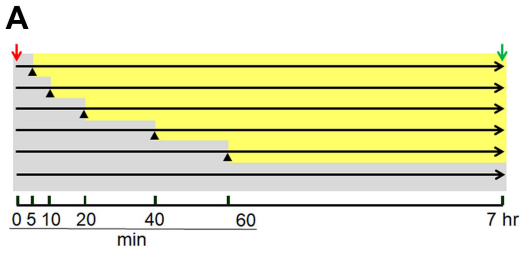
A
0 5 10 20 40 60 7 hr
min

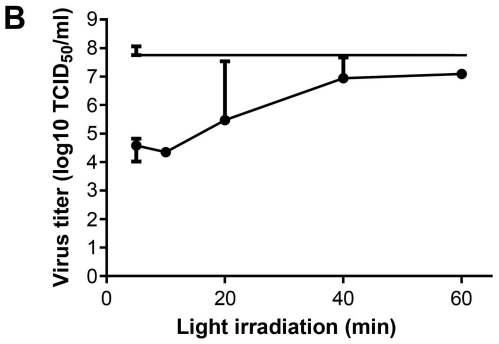
B
Virus titer (log10 TCID50/ml)
Light irradiation (min)

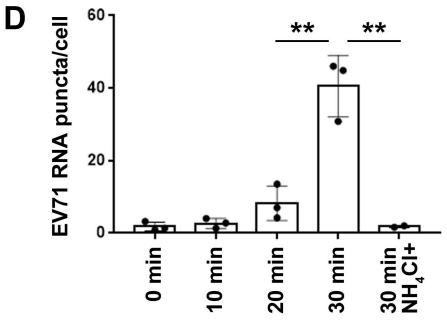
D
EV71 RNA puncta/cell
**
**
0 min
10 min
20 min
30 min
30 min NH4Cl+

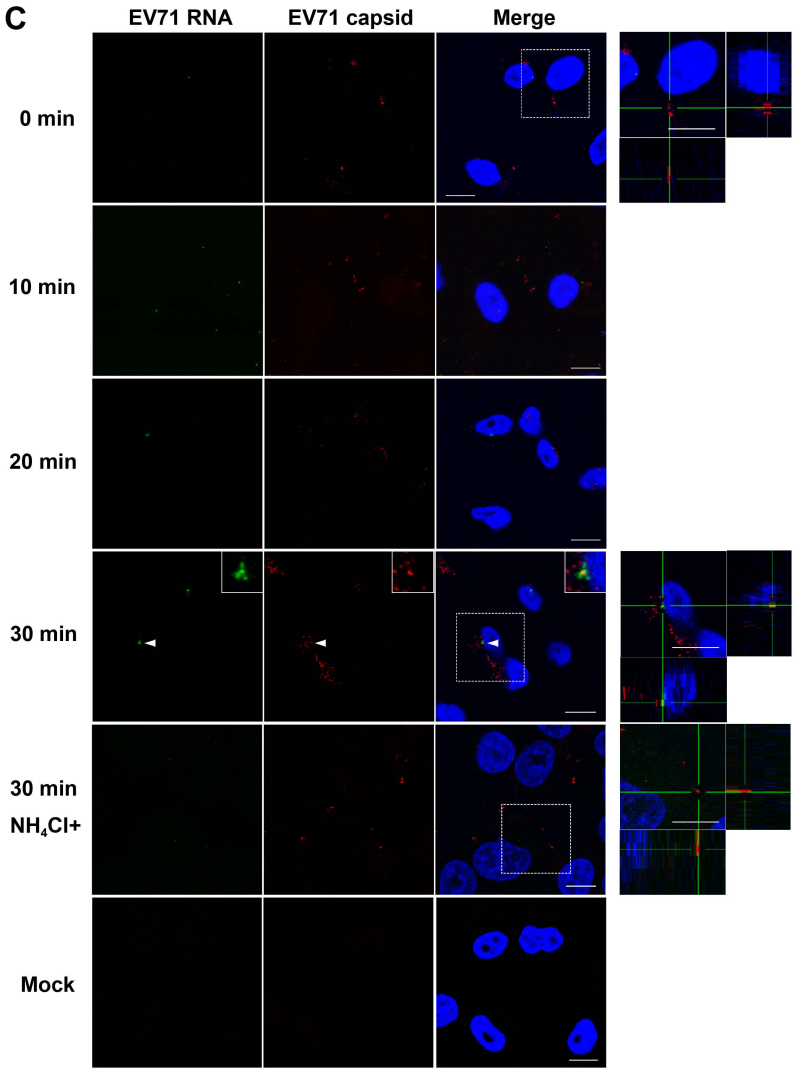
C
EV71 RNA
EV71 capsid
Merge
0 min
10 min
20 min
30 min
30 min NH4Cl+
Mock

Figure 2

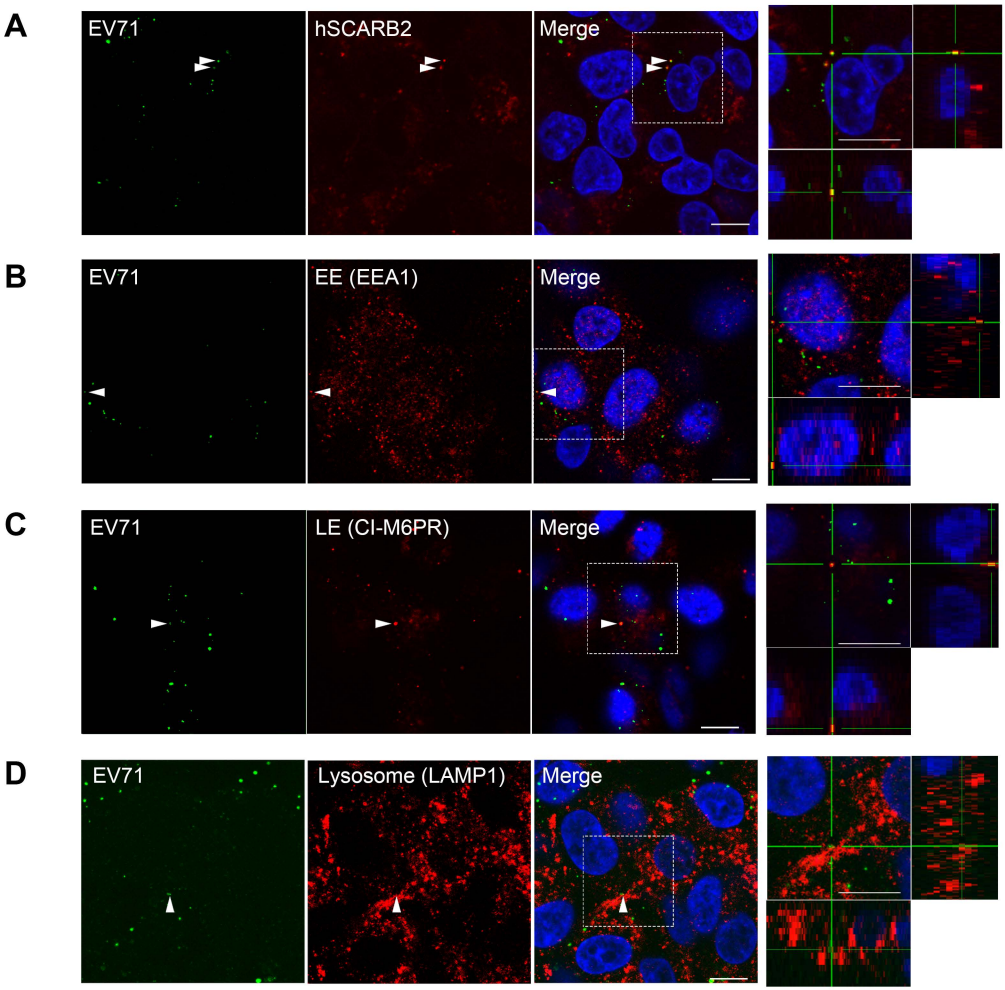
A
EV71
hSCARB2
Merge
B
EV71
EE (EEA1)
Merge
C
EV71
LE (CI-M6PR)
Merge
D
EV71
Lysosome (LAMP1)
Merge

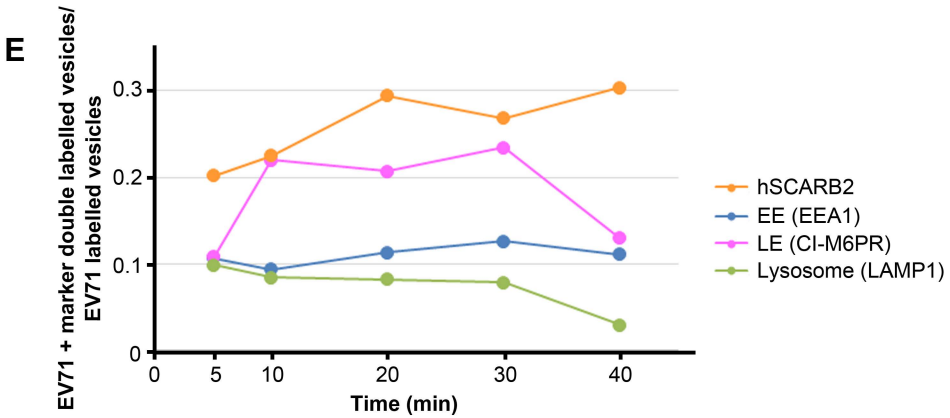
E
EV71 + marker double labelled vesicles/
EV71 labelled vesicles
0.3
0.2
0.1
0
0
5
10
20
30
40
Time (min)
hSCARB2
EE (EEA1)
LE (CI-M6PR)
Lysosome (LAMP1)

Figure 3

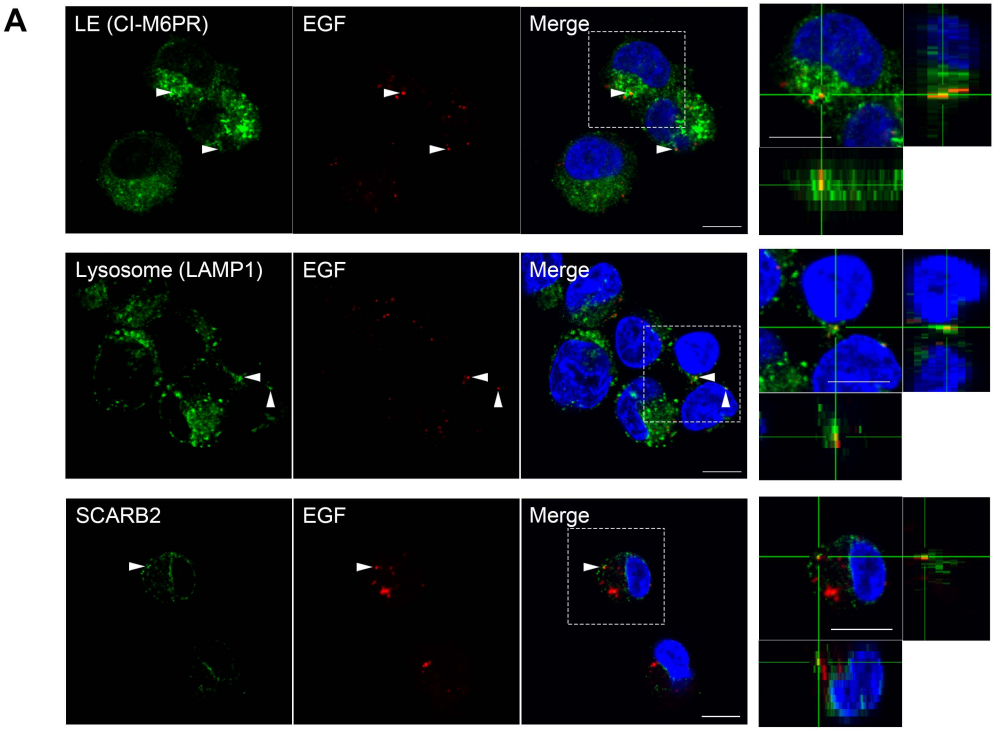
A
LE (CI-M6PR)
EGF
Merge
Lysosome (LAMP1)
EGF
Merge
SCARB2
EGF
Merge
B
EGF + marker double labelled vesicles/
EGF labelled vesicles
0.6
0.4
0.2
0
ns
**
LE
(CI-M6PR)
Lysosome
(LAMP1)
SCARB2

Figure 4

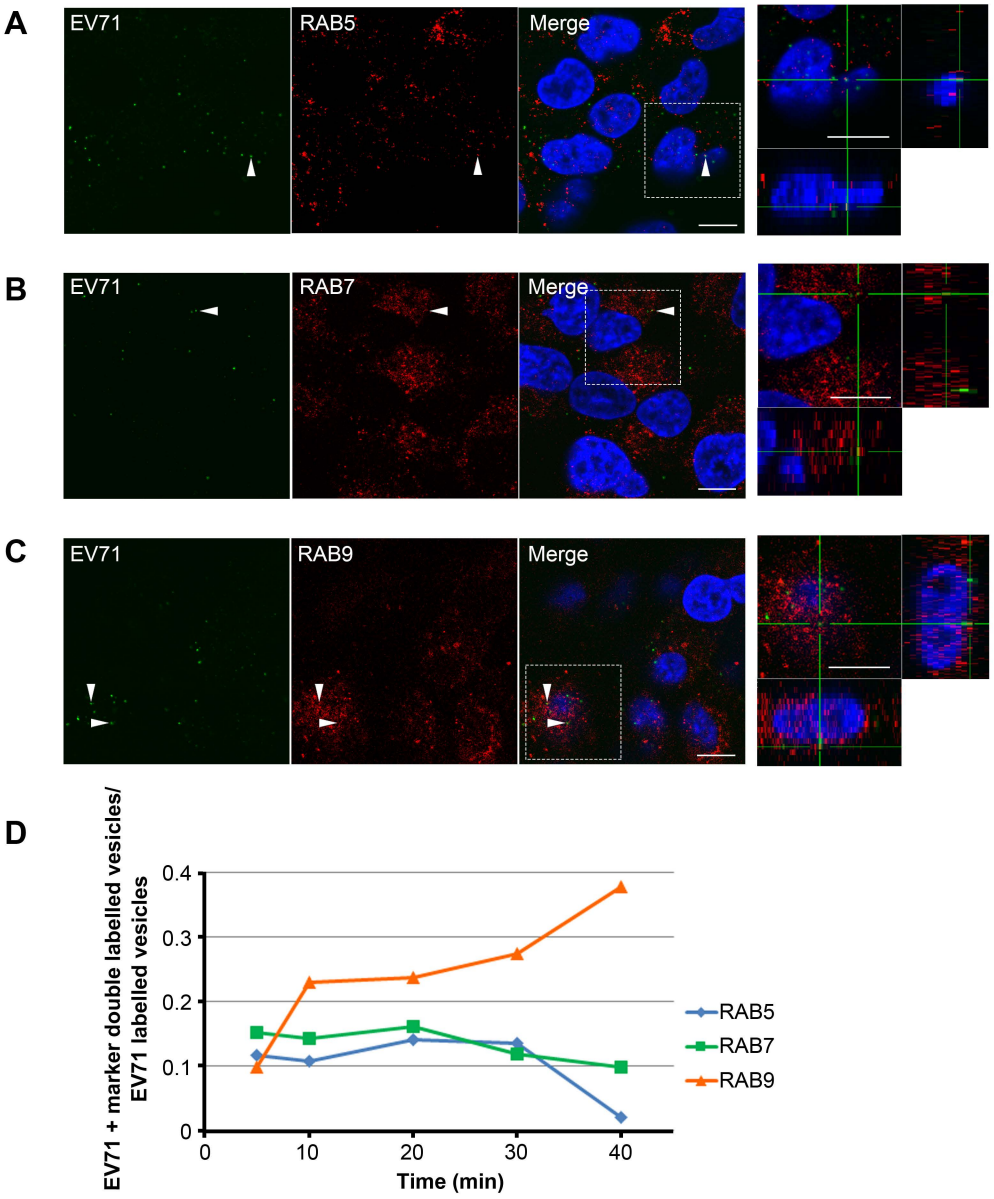
A
EV71
RAB5
Merge
B
EV71
RAB7
Merge
C
EV71
RAB9
Merge
D
EV71 + marker double labelled vesicles/
EV71 labelled vesicles
0.4
0.3
0.2
0.1
0
0
10
20
30
40
Time (min)
RAB5
RAB7
RAB9

Figure 5

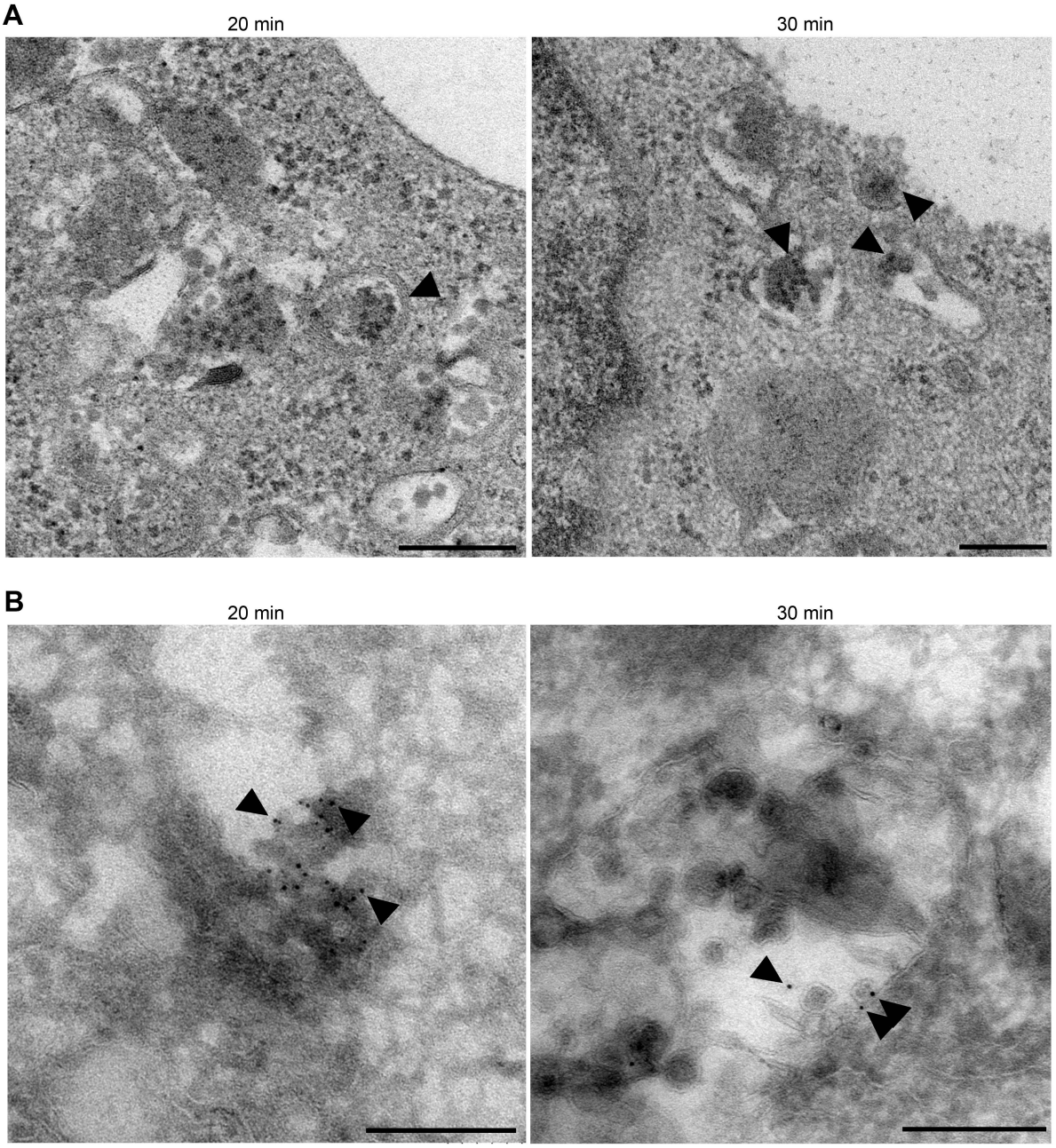

Figure 6

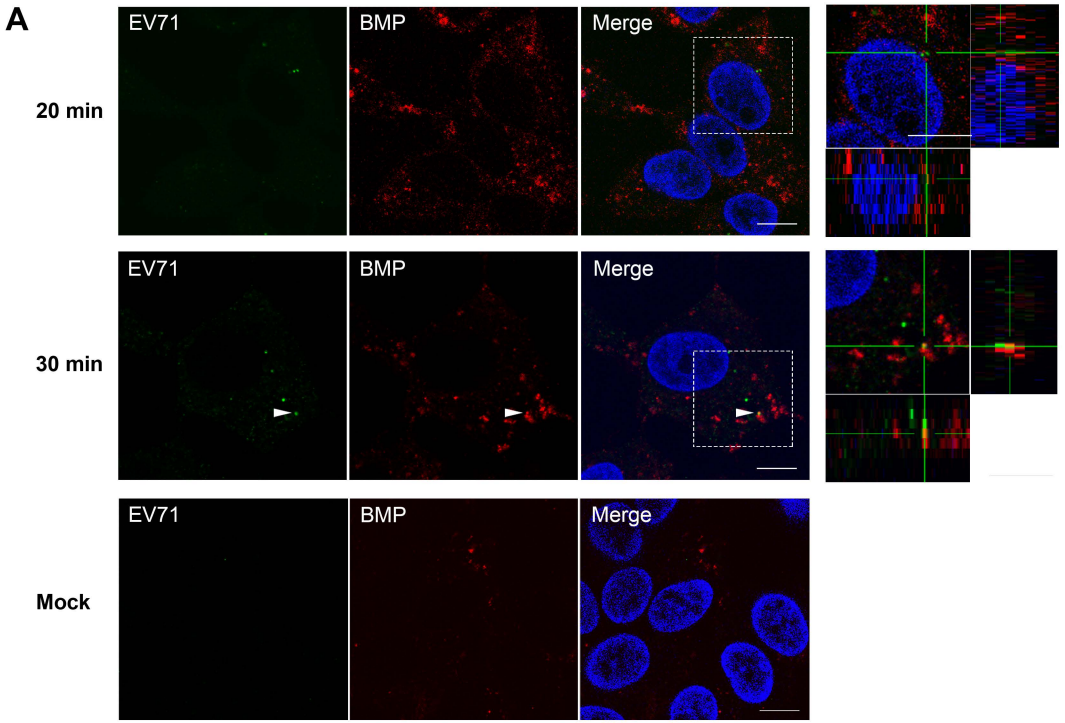
A
20 min
30 min
Mock
EV71
BMP
Merge
B
EV71 + BMP
double labelled vesicles/
EV71 labelled vesicles
0.5
0.4
0.3
0.2
0.1
0
**
20
30
Time (min)

Figure 7

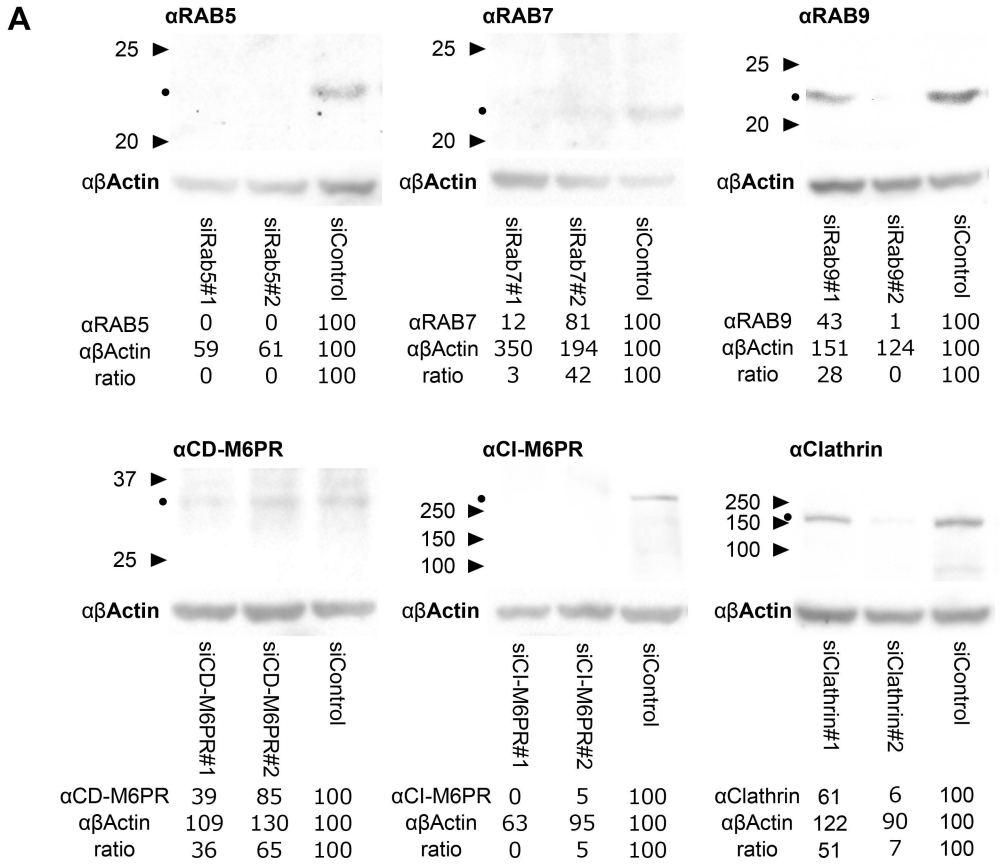
A
αRAB5
25
20
αβActin
siRab5#1
siRab5#2
siControl
αRAB5 0 0 100
αβActin 59 61 100
ratio 0 0 100
αRAB7
25
20
αβActin
siRab7#1
siRab7#2
siControl
αRAB7 12 81 100
αβActin 350 194 100
ratio 3 42 100
αRAB9
25
20
αβActin
siRab9#1
siRab9#2
siControl
αRAB9 43 1 100
αβActin 151 124 100
ratio 28 0 100
αCD-M6PR
37
25
αβActin
siCD-M6PR#1
siCD-M6PR#2
siControl
αCD-M6PR 39 85 100
αβActin 109 130 100
ratio 36 65 100
αCI-M6PR
250
150
100
αβActin
siCI-M6PR#1
siCI-M6PR#2
siControl
αCI-M6PR 0 5 100
αβActin 63 95 100
ratio 0 5 100
αClathrin
250
150
100
αβActin
siClathrin#1
siClathrin#2
siControl
αClathrin 61 6 100
αβActin 122 90 100
ratio 51 7 100

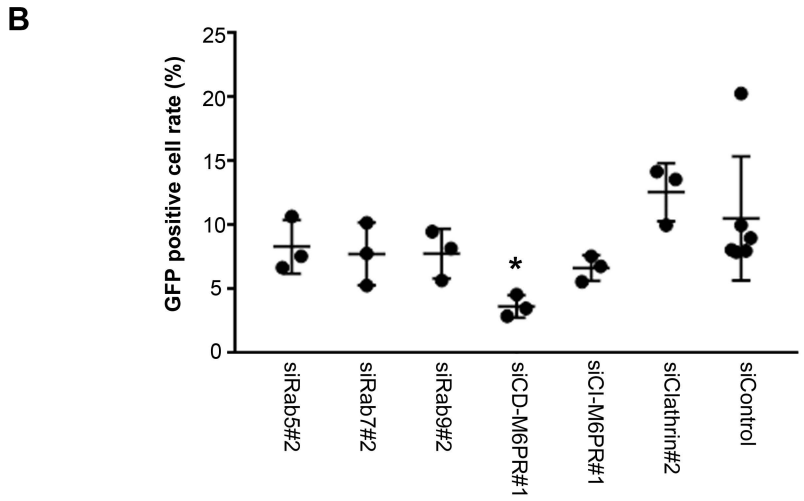
B
GFP positive cell rate (%)
25
20
15
10
5
0
*
siRab5#2
siRab7#2
siRab9#2
siCD-M6PR#1
siCI-M6PR#1
siClathrin#2
siControl

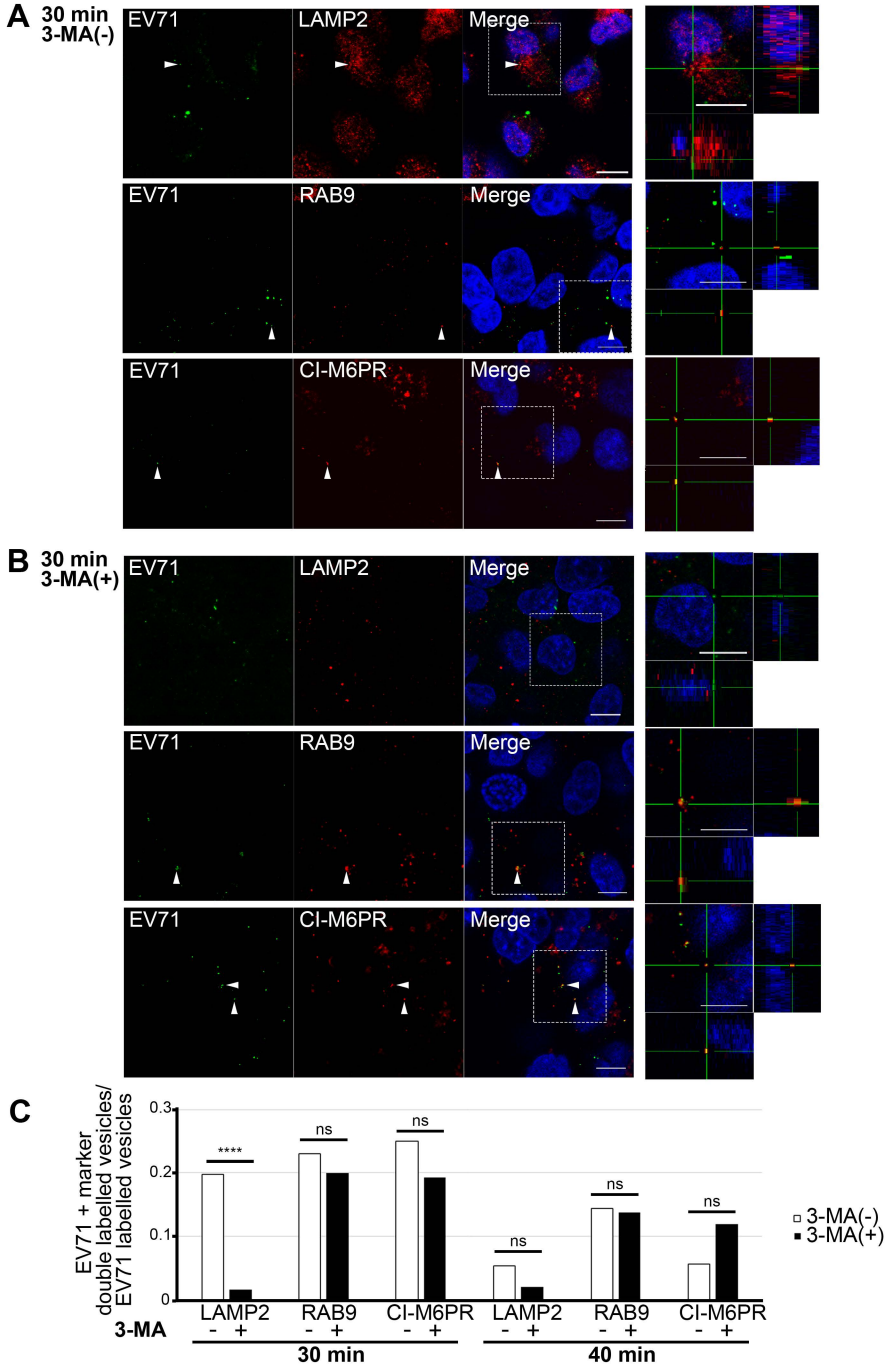

Supplementary Figure S1. 3-MA does not significantly alter the co-localization of EV71 with RAB9 or M6PR
(A, B) RD-hSCARB2 cells were infected with EV71 without (A) or with 3-MA (B) and cells were fixed 30 minutes after the infection followed by immunofluorescence to detect EV71 and LAMP2, RAB9, or M6PR. DAPI is in blue, EV71 antigen is in green, whereas LAMP2, RAB9, or M6PR are in red. The panels on the right are enlarged merge 3D cross-section views of the dashed rectangles in the merged panels. Arrowheads indicate co-localization of EV71 with markers. Representative images are shown. Scale bar, 10 μm. (C) Kinetics of co-localization of EV71 with the different markers. Times indicate the time after infection. ****, $P < 0.0001$, ns, not significant. Statistical significance was determined by a two-tailed, Fisher's exact test.

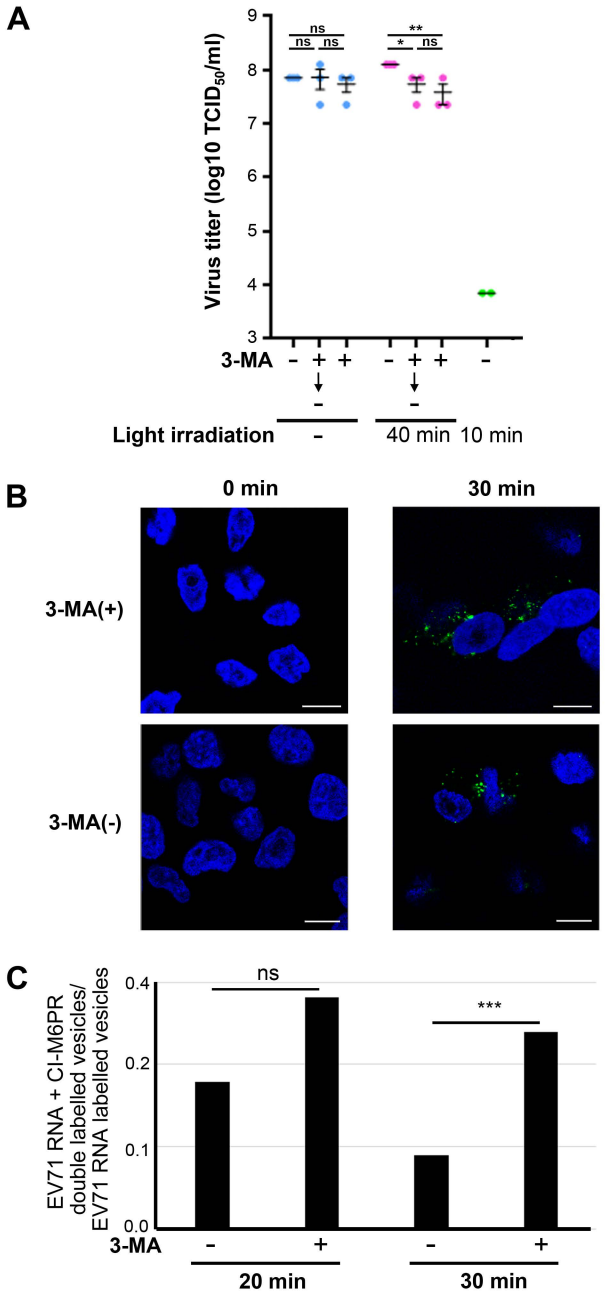

Supplementary Figure S2. 3-MA does not block EV71 uncoating
(A) Effect of 3-MA on EV71 uncoating using light-sensitive EV71. RD-hSCARB2 cells were infected with light-sensitive EV71 in the absence (3-MA (-)) or presence (3-MA (+)) of 3-MA. "3-MA (+) to (-)" indicates that the medium with 3-MA were changed to standard medium after the light irradiation. Infected cells were kept in the dark or irradiated with light at 10 or 40 m.a.i. to inactivate intact virus. 23 hours after the infection, cells were harvested and viral titers were determined. Error bars represent s.d.; ns, not significant, *, $P < 0.05$, **, $P < 0.01$. Statistical significance was determined by a two-tailed, unpaired t-test. (B) In situ hybridization for RNA genome of EV71 to detect uncoating of the virus. DAPI is in blue, whereas EV71 RNA genome is in green. Representative images are shown. Scale bar, 10 μm. (C) Ratio of EV71 with M6PR vesicles/EV71 vesicles are shown. ns, not significant, ***, $P = 0.0001$. Statistical significance was determined by a two-tailed, Fisher' s exact test.

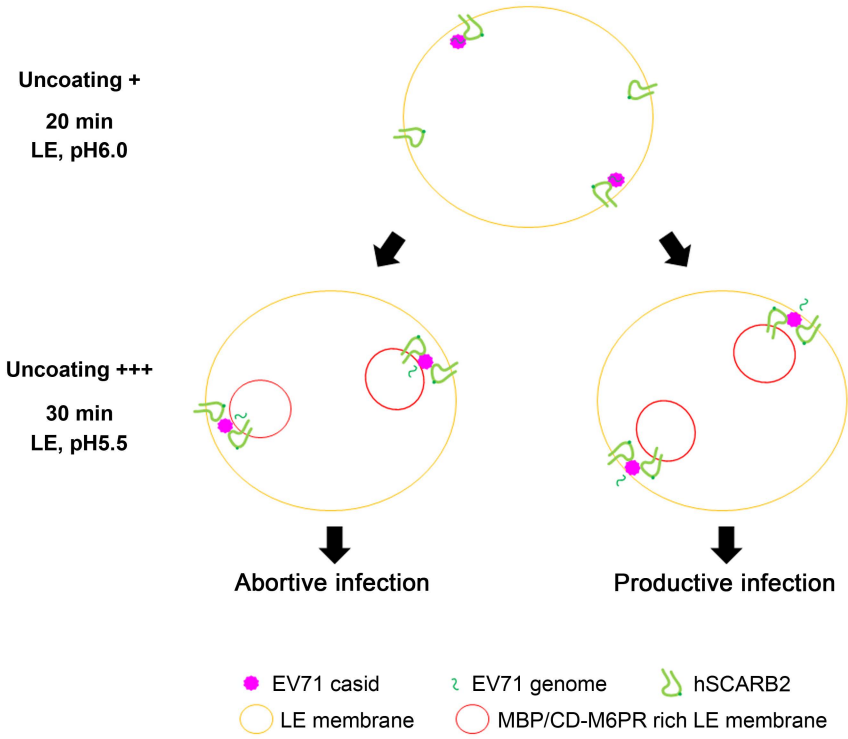

Supplementary Figure S3. Possible mechanisms for EV71 uncoating and abortive infection
At 20 m.a.i., EV71 exists in LEs containing low BMP, with less ILVs and higher pH. At 30 m.a.i., LEs with more ILVs containing EV71 accumulate BMP and are acidified, leading to EV71 uncoating. When EV71 uncoating occurs on the ILVs, viral RNAs reside inside the LEs, resulting to abortive infection.